Revisiting the Capacity of Noncoherent Fading Channels in mmWave System

Guido C. Ferrante°⋆, Tony Q. S. Quek° and Moe Z. Win⋆
°Singapore University of Technology and Design, Singapore
⋆Massachusetts Institute of Technology, MA, USA

***Abstract*—Millimeter wave communications will use large bandwidth and experience severe attenuation due to the pathloss. The two above conditions may force the communication system to enter the so-called *wideband regime*, where transmitted signals must be increasingly "peaky" in order to achieve a large fraction of the wideband capacity. This paper investigates noncoherent capacity of millimeter wave communications with average and peak power constrained inputs as a function of bandwidth. The impact of several parameters, in particular coherence block size and strength of the normalized specular component in line-of-sight propagation, is also studied. Capacity upper and lower bounds are provided and suggest that in practical scenarios the communication system may have to operate in the wideband regime. Paired with non-line-of-sight propagation, dense signaling is shown to limit the maximum achievable rate for typical users in the cell.**

***Index Terms*—Noncoherent capacity, mmWave spectrum, wideband channels.**

I. Introduction

Millimeter wave (mmWave) communications have been recently proposed as a key enabling technology for 5G [1], [2]. Thanks to the large bandwidth, mmWave communications promise to offer data rates more than one order of magnitude higher than LTE [3]. However, propagation at mmWave frequencies is peculiar. Recent measurement campaigns show the presence of blockages, severe attenuation due to higher carrier frequencies, and significant non-line-of-sight (NLOS) propagation [3]–[5]. Channel capacity for channels accounting for the above properties has not yet been investigated.

The maximum rate achievable in fading channels is provided by the *noncoherent capacity*. In particular, the wideband capacity limit for the additive white Gaussian noise (AWGN) channel is not representative of the wideband capacity limit for fading channels, especially when inputs are peak constrained (dense signaling). Without the peak constraint assumption, the noncoherent wideband capacity limit is equal to the AWGN wideband capacity limit, that is $\mathcal{P}/\mathcal{N}_0$ nats/s, where $\mathcal{P}$ is the power of the received signal and $\mathcal{N}_0$ is the noise spectral height, a result that dates back to Pierce [6] and Kennedy [7]. However, the required signaling is increasingly "peaky" [8] for the above result to hold. In full generality, Verdú showed that signaling has to be *flash* [9], *i.e.*, the input distribution must be increasingly concentrated about a zero-cost input as bandwidth increases, while satisfying the average power constraint with equality by exhibiting a small component at large amplitude values. In our setting, the cost of the communication is the power and the zero-cost input is mapped to a waveform that is equal to zero. Peak constraint is often required in practice, hence the noncoherent capacity investigation with peak-constrained input is valuable for concrete applications.

Recent literature on noncoherent capacity can be classified on the basis of the channel model and the signal-to-noise ratio (SNR) regime of interest. Following the first criterion, channels were mainly modeled according to either block models [10]–[14] or stationary models [8], [15]–[19], that represent the two extrema corresponding to "discontinuous" (or "abrupt") vs. "continuous" (or "smooth") fading correlation across signal space dimensions. According to the second criterion, capacity bounds were typically derived with a focus on either the high-SNR regime [16], [17] or the low-SNR regime [8], [9], [12], [13], [18]. Capacity wideband scaling was first investigated in [8], [20] in relation to a wide-sense stationary uncorrelated-scattering (WSSUS) fading channel. It was shown that capacity of signals with second and fourth moment constraints proportional to $1/\mathcal{W}$ and $1/\mathcal{W}^2$, respectively, where $\mathcal{W}$ is the bandwidth of the signal, scales as $1/\mathcal{W}$. The fourth moment constraint guarantees that transmitted signals spread energy "evenly" on signal space dimensions. A similar behavior was shown in [21] for multipath channels and "white-like" signals. Differently from above, capacity bounds as a function of bandwidth $\mathcal{W}$ for fixed power $\mathcal{P}$ were presented in [19], under both average power and amplitude constraints, in a Rayleigh-fading WSSUS channel: the analysis in this case covered both high- and low-SNR regimes.

In this paper we derive capacity bounds as a function of bandwidth similarly as [19]. Differently from [19], we introduce mmWave channel features, namely blockages, line-of-sight (LOS) propagation and power profile in frequency due to water and oxygen absorption, and model the channel according to a block-fading model. We study capacity with either amplitude or fourth-moment constrained inputs. We derive explicit capacity lower bounds and show achievable rates of practical signaling schemes based on training. We discuss the impact of several system parameters, in particular coherence block size and LOS path strength, on achievable rates, and present numerical results for a scenario of interest based on the recent measurement campaign [3].

II. System Model

We assume that a baseband signal of duration $\mathcal{T}$ and bandwdith $\mathcal{W}$ is transmitted over a doubly dispersive channel having coherence time $\mathcal{T}_{\text{coh}}$ and coherence bandwidth $\mathcal{W}_{\text{coh}}$

(see Fig. 1). We consider a Weyl-Heisenberg (or Gabor) set $\{\phi_{kl}(t) := g(t-kT)e^{j2\pi lW}\}$, with $t \mapsto g(t)$ a baseband bandlimited function. One can think of $\phi_{kl}(t)$ as a signal that is "well localized" in the time-frequency plane around (kT, lW) and occupies a unit-area rectangle of duration T and bandwidth W (refer to [19] for the details). Denote T_{d} the delay spread and W_{D} the Doppler spread of the channel. The following relations hold in a dense scattering environment: $\mathcal{W}_{\mathrm{coh}} = 1/T_{\mathrm{d}}$; $\mathcal{T}_{\mathrm{coh}} = 1/W_{\mathrm{D}}$. It turns out that, for typical scenarios, mmWave channels are underspread, that is, $T_{\mathrm{d}}W_{\mathrm{D}} \ll 1$, hence each coherence block has dimension $(\mathcal{T}_{\mathrm{coh}}\mathcal{W}_{\mathrm{coh}})/(TW) \gg 1$ once discretized. Parameters T and W can be chosen according to a *matched design*, that is $T/W = T_{\mathrm{d}}/W_{\mathrm{D}}$ [19], [22]. Projection onto the Weyl-Heisenberg set maps the continuous-time channel onto a set of parallel flat-fading channels

$$\mathsf{y}_{kl} = \mathsf{h}_{kl}\mathsf{x}_{kl} + \mathsf{n}_{kl},\ 0 \leqslant k \leqslant K-1,\ 0 \leqslant l \leqslant L-1, \quad (1)$$

where: x_{kl} and y_{kl} are the transmitted and received signals projected onto ϕ_{kl}; h_{kl} is the channel coefficient; n_{kl} is the unit-variance additive white Gaussian noise; $K = \mathcal{T}/T$ and $L = \mathcal{W}/W$ (for the sake of simplicity, we assume K and L integers). We organize (1) in matrix form as follows,

$$\mathsf{Y} = \mathsf{H} \odot \mathsf{X} + \mathsf{N}, \quad (2)$$

where $\odot$ is the Hadamard (elementwise) product, $[\mathsf{Y}]_{kl} = \mathsf{y}_{kl}$, and H, X and N similarly defined. We assume a block-fading model, that is, the channel is assumed constant over each coherence block, and channel coefficients are independent across blocks. Formally, denote $D_{\mathsf{T}} = \mathcal{T}/\mathcal{T}_{\mathrm{coh}}$ and $D_{\mathsf{W}} = \mathcal{W}/\mathcal{W}_{\mathrm{coh}}$ the number of coherence blocks in time and frequency, respectively, and H_{ij} the fading coefficient within coherence block (i,j), with $1 \leqslant i \leqslant D_{\mathsf{T}}$ and $1 \leqslant j \leqslant D_{\mathsf{W}}$. That is, $H_{ij} := [\mathsf{H}]_{(i-1)\ell_{\mathsf{T}}+k,(j-1)\ell_{\mathsf{W}}+l}$ for all $0 \leqslant k \leqslant \ell_{\mathsf{T}}-1$ and $0 \leqslant l \leqslant \ell_{\mathsf{W}}-1$, having denoted $\ell_{\mathsf{T}} = K/D_{\mathsf{T}} = \mathcal{T}_{\mathrm{coh}}/T$, and $\ell_{\mathsf{W}} = L/D_{\mathsf{W}} = \mathcal{W}_{\mathrm{coh}}/W$. For brevity, we will denote $\ell = \ell_{\mathsf{T}}\ell_{\mathsf{W}}$ the block size.

Three properties peculiar of mmWave propagation channels are taken into account, namely blockages, power absorption profile, and LOS/NLOS fading [3]. Hence, we propose to model channel coefficient H_{ij} as

$$H_{ij} = A_i v_j G_{ij}, \quad (3)$$

where: $A_i \sim \mathrm{Bernoulli}(1-p_{\mathrm{B}})$ accounts for blockages at coherence time i, where p_{B} is the probability of blockage; v_j is deterministic and approximates the absorption at coherence band j; and $G_{ij} \sim \mathcal{CN}(\mathsf{k}, 1-|\mathsf{k}|^2)$ accounts for the Rician fading in block (i,j). The channel block structure induces a natural partition of matrices in (2). Let Y_{ij} be the $\ell_{\mathsf{T}} \times \ell_{\mathsf{W}}$ matrix of the received signal in coherence block (i,j), and similarly define H_{ij}, X_{ij}, and N_{ij}. The relation between blocks is $\mathsf{Y}_{ij} = \mathsf{H}_{ij} \odot \mathsf{X}_{ij} + \mathsf{N}_{ij} = H_{ij}\mathsf{X}_{ij} + \mathsf{N}_{ij}$. Vectorizing each block, that is, defining $\boldsymbol{Y}_{ij} = \mathrm{vec}(\mathsf{Y}_{ij})$ and using similar notations for $\boldsymbol{H}_{ij}$, $\boldsymbol{X}_{ij}$, and $\boldsymbol{N}_{ij}$, yields $\boldsymbol{Y}_{ij} = \boldsymbol{H}_{ij} \odot \boldsymbol{X}_{ij} + \boldsymbol{N}_{ij} = H_{ij}\boldsymbol{X}_{ij} + \boldsymbol{N}_{ij}$. Stacking vectors in j first and then in i yields an equivalent vector form of (2):

$$\boldsymbol{Y} = \boldsymbol{H} \odot \boldsymbol{X} + \boldsymbol{N}. \quad (4)$$

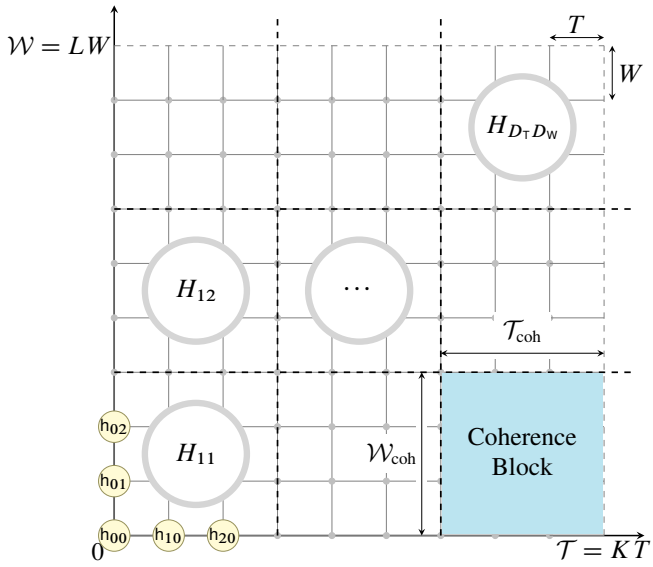

FIG. 1: Representation of the doubly-dispersive block-fading model.

The problem statement is as follows: find the noncoherent capacity of channel (4),

$$C = \frac{1}{\mathcal{T}} \sup_{P_{\mathsf{X}}} I(\boldsymbol{X};\boldsymbol{Y}), \quad (5)$$

when input distributions satisfy an *average power constraint*,

$$\frac{1}{\mathcal{T}}\,\mathbb{E}[\,\|\boldsymbol{X}\|_2^2\,] \leqslant \mathcal{P} =: P\mathcal{W}, \quad (6)$$

where $\mathcal{P}$ is the received power and P is the received power per degree of freedom, and a *peak power constraint* in the form of either *amplitude constraint*,

$$|[\mathsf{X}]_{kl}|^2 \leqslant \beta\frac{\mathcal{P}}{\mathcal{W}} = \beta P \quad \text{a.s.}, \quad (7)$$

or *fourth-moment constraint*,

$$\mathbb{E}[\,|[\mathsf{X}]_{kl}|^4\,] \leqslant \beta P^2, \quad (8)$$

for $0 \leqslant k \leqslant K-1$ and $0 \leqslant l \leqslant L-1$. Note that eqs. (6) and (7) can be compactly rewritten $\mathbb{E}[\,\|\boldsymbol{X}\|_2^2\,] \leqslant KLP$ and $\|\boldsymbol{X}\|_\infty^2 \leqslant \beta P$ a.s., respectively.

III. Capacity Upper Bounds

In this section we present three Theorems stating capacity upper bounds. Due to space constraints, proofs are omitted and will be presented in a journal version of this paper.

In the below Theorem 1 we derive an upper bound without taking into account any peak constraint. It proves to be useful in the high-SNR regime.

Theorem 1. *Consider a block-fading channel with D_{T} coherent blocks in of dimension ℓ_{T} and D_{W} coherent blocks in frequency of dimension ℓ_{W}. Assume that the absorption profile is $(v_1,\ldots,v_{D_{\mathsf{W}}})$, the blockage probability is p_{B}, and inputs are subject to the average power constraint $\mathbb{E}[\,\|\boldsymbol{X}\|_2^2\,] \leqslant KLP$. Denote $P_j^\star = [p(v_j,\lambda)]^+$, where $p(v,\lambda)$ is the solution of*

$[1-\psi(vp)]+p\lambda=0$, *and* $\psi(\xi)=\mathbb{E}[\,1/(1+\xi|g|^2)\,]$. *An upper bound to capacity is*

$$\sup_{P_{\boldsymbol{X}}}\frac{1}{KL}I(\boldsymbol{X};\boldsymbol{Y})\leqslant(1-p_{\mathrm{B}})\frac{1}{D_{\mathsf{W}}}\sum_{j=1}^{D_{\mathsf{W}}}\mathcal{J}(v_j^2P_j^\star),\qquad(9)$$

where $\mathcal{J}(\xi)=\mathbb{E}[\,\log(1+|g|^2\xi)\,]$, *and* λ *is such that the average power constraint is satisfied with equality, i.e.,* $\sum_{j=1}^{D_{\mathsf{W}}}P_j^\star(\lambda)=D_{\mathsf{W}}P$.

The power allocation is strictly related to mercury/water-filling [23], [24]. In general, ψ is not available in closed form, and the problem is numerically solved. In the below Corollary 1 we explicit the case with no absorption, *i.e.*, $v_1=\cdots=v_{D_{\mathsf{W}}}=1$, where the optimum power allocation can be found in closed form.

Corollary 1. *Let the assumptions be as in Theorem 1 and set* $v_1=\cdots=v_{D_{\mathsf{W}}}=1$. *Capacity is upper bounded as*

$$\sup_{P_{\boldsymbol{X}}}\frac{1}{KL}I(\boldsymbol{X};\boldsymbol{Y})\leqslant(1-p_{\mathrm{B}})\mathcal{J}(P)\qquad(10)$$

where $\mathcal{J}(\xi)=\mathbb{E}[\,\log(1+|g|^2\xi)\,]$.

We present an upper bound with amplitude constrained inputs in the below Theorem 2, that is obtained by adapting the bounding idea of [19] to block-fading channels, and simplify the bound in the case of no absorption in Corollary 2.

Theorem 2. *Let the assumptions be as in Theorem 1 and let inputs be further subject to the amplitude constraint* $\|\boldsymbol{X}\|_\infty^2\leqslant\beta P$. *Capacity is upper bounded as*

$$\sup_{P_{\boldsymbol{X}}}\frac{1}{KL}I(\boldsymbol{X};\boldsymbol{Y})\leqslant\frac{1-p_{\mathrm{B}}}{D_{\mathsf{W}}}\sup_{q\in[0,1]}\Bigg\{\sum_{j=1}^{D_{\mathsf{W}}}\log(1+v_j^2P_j^\star)-\frac{qP}{\ell P_{\mathrm{sum}}^\circ}\log(1+v_j^2\ell P_j^\circ(1-|\mathsf{k}|^2))\Bigg\}\qquad(11)$$

where $P_j^\star=(\lambda-1/v_j^2)^+$ *with* λ *such that* $\sum_{j=1}^{D_{\mathsf{W}}}P_j^\star=qD_{\mathsf{W}}P$, *and* $P_{\mathrm{sum}}^\circ=P_1^\circ+\cdots+P_{D_{\mathsf{W}}}^\circ$, *being*

$$(P_1^\circ,\cdots,P_{D_{\mathsf{W}}}^\circ)=\underset{\substack{(P_1,\cdots,P_{D_{\mathsf{W}}})\\\in\{0,\beta P\}^{D_{\mathsf{W}}}}}{\operatorname{argmin}}\sum_{j=1}^{D_{\mathsf{W}}}\frac{\log(1+v_j^2\ell P_j(1-|\mathsf{k}|^2))}{P_1+\cdots+P_{D_{\mathsf{W}}}}.$$

Corollary 2. *Let the assumptions be as in Theorem 2 and set* $v_1=\cdots=v_{D_{\mathsf{W}}}=1$. *Capacity is upper bounded as*

$$\sup_{P_{\boldsymbol{X}}}\frac{1}{KL}I(\boldsymbol{X};\boldsymbol{Y})\leqslant(1-p_{\mathrm{B}})\sup_{q\in[0,1]}\Bigg\{\log(1+qP)-\frac{q}{\beta\ell}\log\Big(1+\beta\ell P(1-|\mathsf{k}|^2)\Big)\Bigg\}.\qquad(12)$$

When the peak power constraint is the fourth-moment constraint, similar results hold, as shown in the below Theorem 3 and Corollary 3.

Theorem 3. *Let the assumptions be as in Theorem 1 and let inputs be further subject to the fourth-moment constraint* $\mathbb{E}[\,|[\mathsf{X}]_{kl}|^4\,]\leqslant\beta P^2$. *Capacity is upper bounded as*

$$\sup_{P_{\boldsymbol{X}}}\frac{1}{KL}I(\boldsymbol{X};\boldsymbol{Y})\leqslant\frac{1-p_{\mathrm{B}}}{D_{\mathsf{W}}}\sup_{q\in[0,1]}\Bigg\{\sum_{j=1}^{D_{\mathsf{W}}}\Bigg[\log(1+\tilde{v}_j^2P_j^\star)-\frac{1}{D_{\mathsf{T}}}\sum_{i=1}^{D_{\mathsf{T}}}\frac{q^2\bar{P}_{ij}^2}{\ell\beta P^2}\log\Big(1+v_j^2(1-|\mathsf{k}|^2)\frac{\ell\beta P^2}{q\bar{P}_{ij}}\Big)\Bigg]\Bigg\}\qquad(13)$$

with $P_j^\star=(\lambda-1/v_j^2)^+$, λ *such that* $\sum_{j=1}^{D_{\mathsf{W}}}P_j^\star=qD_{\mathsf{W}}P$, *and*

$$\{\bar{P}_{ij}\}_{ij}=\underset{\substack{0\leqslant P_{ij}\leqslant\sqrt{\beta}P\\\sum_{ij}P_{ij}=D_{\mathsf{T}}D_{\mathsf{W}}P}}{\operatorname{arginf}}\sum_{i=1}^{D_{\mathsf{T}}}\sum_{j=1}^{D_{\mathsf{W}}}\frac{q^2P_{ij}^2}{\beta P^2}\log\Big(1+v_j^2(1-|\mathsf{k}|^2)\frac{\ell\beta P^2}{qP_{ij}}\Big).$$

Corollary 3. *Let the assumptions be as in Theorem 3 and set* $v_1=\cdots=v_{D_{\mathsf{W}}}=1$. *Capacity is upper bounded as follows:*

$$\sup_{P_{\boldsymbol{X}}}\frac{1}{KL}I(\boldsymbol{X};\boldsymbol{Y})\leqslant(1-p_{\mathrm{B}})\sup_{q\in[0,1]}\Bigg\{\log(1+qP)-\frac{q^2}{\ell\beta}\log\Big(1+(1-|\mathsf{k}|^2)\frac{\ell\beta P}{q}\Big)\Bigg\}\qquad(14)$$

Remark 1. Both results in Corollary 2 and 3 have same expansion as $P\to0$ equal to $(1-p_{\mathrm{B}})|\mathsf{k}|^2P$. It can be shown that, in the NLOS scenario, capacity (bits/s) is proportional to $1/\mathcal{W}$, in line with [8].

IV. Capacity Lower Bounds

In this section, we assume independent inputs over different coherence blocks, that yields

$$I(\boldsymbol{X};\boldsymbol{Y})=\sum_{i=1}^{D_{\mathsf{T}}}\sum_{j=1}^{D_{\mathsf{W}}}I(\boldsymbol{X}_{ij};\boldsymbol{Y}_{ij}),\qquad(15)$$

and derive bounds for the mutual information in the generic block, *i.e.*, $I(\boldsymbol{X}_{ij};\boldsymbol{Y}_{ij})$. The average power allocated to each block can be later optimized via mercury/water-filling [23], [24] on the basis of the sole knowledge of $\{v_1,\ldots,v_{D_{\mathsf{W}}}\}$. For notation simplicity, we drop subscripts and denote $I(\bar{\boldsymbol{X}};\bar{\boldsymbol{Y}})$ the mutual information in the generic block, and $\bar{X}$ the generic element of $\bar{\boldsymbol{X}}$.

Lemma 1. *Consider a block-fading channel where the absorption coefficient of the generic block is* v *and the blockage probability is* p_{B}. *Let inputs be subject to both average power constraint* $\mathbb{E}[\,\|\bar{\boldsymbol{X}}\|_2^2\,]\leqslant\ell P$ *and fourth-moment constraint* $\mathbb{E}[\,|\bar{X}|^4\,]\leqslant\beta P^2$. *An achievable rate per block is*

$$\sup_{P_{\bar{\boldsymbol{X}}}}\frac{1}{\ell}I(\bar{\boldsymbol{X}};\bar{\boldsymbol{Y}})\geqslant(1-p_{\mathrm{B}})\Big[\,\mathbb{E}_{g\sim P_G}[\,h(vg\bar{X}+N)\,]-\log(\pi e)\Big]-\tfrac{1}{\ell}\,\mathbb{E}_{\bar{\boldsymbol{x}}\sim P_{\bar{\boldsymbol{X}}}}[\,\log(1+\sigma_H^2\|\bar{\boldsymbol{x}}\|_2^2)\,]\qquad(16)$$

for any $P_{\bar{\boldsymbol{X}}}$ *satisfying both power constraints.*

When $\beta\geqslant2$, we can apply Jensen's inequality to the second term in the RHS of (16) and consider the maximum entropy distribution, that is Gaussian, for the remaining term. The result is summarized in the following Corollary.

Corollary 4. *Let the assumptions be as in Lemma 1, and let* $\beta\geqslant2$. *An achievable rate per block is*

$$\sup_{P_{\bar{X}}} \frac{1}{\ell} I(\bar{\boldsymbol{X}};\bar{\boldsymbol{Y}}) \geqslant (1-p_{\mathrm{B}})\, \mathbb{E}_{g\sim P_G}[\log(1+v^2|g|^2 P)\,] - \tfrac{1}{\ell}\log(1+\sigma_H^2 \ell P). \quad (17)$$

As a matter of fact, Corollary 4 is not tight in the peak constraint. We can improve the bound via a time-sharing argument [19], where transmission is allowed over a fraction θ of blocks only. Since blocks can be arbitrarily selected in the time as well as the frequency domain, we refer to it as *block sharing*.

Theorem 4. *Let the assumptions be as in Lemma 1. Denote $\kappa_{\bar{X}}$ the input kurtosis and $R(P,\kappa_{\bar{X}})$ the achievable rate in* (16)*. An achievable rate per block is*

$$\sup_{P_{\bar{X}}} \frac{1}{\ell} I(\bar{\boldsymbol{X}};\bar{\boldsymbol{Y}}) \;\geqslant \sup_{\kappa_{\bar{X}}/\beta \leqslant \theta \leqslant 1} \theta\, R\Big(\frac{P}{\theta}, \frac{\kappa_{\bar{X}}}{\theta}\Big). \quad (18)$$

Using Gaussian inputs yields the following Corollary.

Corollary 5. *Let the assumptions be as in Theorem 4 and let $\beta \geqslant 2$. Denote $R(P)$ the achievable rate in* (17)*. An achievable rate per block is*

$$\sup_{P_{\bar{X}}} \frac{1}{\ell} I(\bar{\boldsymbol{X}};\bar{\boldsymbol{Y}}) \;\geqslant \sup_{2/\beta \leqslant \theta \leqslant 1} \theta\, R\Big(\frac{P}{\theta}\Big). \quad (19)$$

Remark 1 (Geometric interpretation of block sharing argument). Since $\theta R(P/\theta)$ nats/degree-of-freedom can be rewritten as $\theta\mathcal{W} R(\mathcal{P}/(\theta\mathcal{W}))$ nats/s, the supremum in (19) with respect to $\theta \in [\theta_0, 1]$, where $\theta_0 \in (0,1)$, can be interpreted as follows: any rate achievable with bandwidth $\mathcal{W}' \in [\theta_0\mathcal{W}, \mathcal{W}]$ is also achievable with $\mathcal{W}$ via block sharing. In particular, with no peak constraint the rate achievable with bandwidth $\mathcal{W}$ is the "running maximum" rate, that is, the maximum rate achievable up to bandwidth $\mathcal{W}$. □

Other achievable rates can be obtained with practical schemes using training. Due to space constraints we omit their discussion here and show in the next section numerical results for two particular cases, namely truncated Gaussian and constant-modulus inputs.

V. Numerical Examples

We consider three different values of $\mathcal{P}/\mathcal{N}_0$ derived from scenarios based on experimental campaigns [3], [5]:

- **Case 1** (user near base station): $\mathcal{P}/\mathcal{N}_0 = 2.09\cdot 10^9$ s^{-1}.
- **Case 2** (user in typical location): $\mathcal{P}/\mathcal{N}_0 = 2.32\cdot 10^7$ s^{-1}.
- **Case 3** (user near cell edge): $\mathcal{P}/\mathcal{N}_0 = 4.13\cdot 10^6$ s^{-1}.

We assume $\mathcal{N}_0 = k_{\mathrm{B}}T = 4.14\cdot 10^{-21}$ joules, where k_{B} is the Boltzmann constant and $T = 300$ kelvin. Values of $\mathcal{P}/\mathcal{N}_0$ can be read in terms of wideband capacity limit of AWGN and fading channels with no peak constraint, *i.e.*, $C_{\mathrm{WB}} = \mathcal{P}/\mathcal{N}_0$ nats/s. In the presence of blockages, the maximum achievable rate is reduced to $(1-p_{\mathrm{B}})C_{\mathrm{WB}}$, that corresponds to approximately 3 Gb/s (Case 1), 30 Mb/s (Case 2), and 1.8 Mb/s (Case 3).

Scenarios are derived as follows. Denote R and r cell radius and user distance from the base station, respectively, and assume that the base station is located at cell center. Pathloss is computed by adding to the free-space pathloss at distance r and carrier frequency f_{c} an additional attenuation $\mathsf{A} = \mathsf{A}(r, f_{\mathrm{c}})$ to match experimental data [3]:

$$\mathsf{PL}\ (\mathrm{dB}) = 20\log_{10} r + 20\log_{10} f_{\mathrm{c}} + 20\log_{10}\tfrac{4\pi}{c} + \mathsf{A}, \quad (20)$$

where c is the speed of light. Beamforming gains are summarized in the variable $\mathsf{G} = \mathsf{G}(f_{\mathrm{c}})$ (dB). Assuming transmitted power $\mathcal{P}_{\mathsf{TX}}$ (dBm) and receiver noise figure F (dB), the received power is

$$\mathcal{P}\ (\mathrm{dBm}) = \mathcal{P}_{\mathsf{TX}}\ (\mathrm{dBm}) + \mathsf{G}\ (\mathrm{dB}) - \mathsf{F}\ (\mathrm{dB}) - \tfrac{\mathcal{N}_0}{1\mathrm{J}}\ (\mathrm{dB}). \quad (21)$$

TABLE I: List of parameters defining different scenarios of interest.

	Variable	Case 1	Case 2	Case 3	Unit
R	Cell radius	200	200	200	m
r	User distance from BS	50	150	200	m
p_{B}	Blockage probability	0	0.1	0.7	(pure)
k	LOS component	0.8	0.2	0	(pure)
A	Additional attenuation	15	25	30	dB
f_{c}	Carrier frequency	73	73	73	GHz
G	Beamforming gain	15	15	15	dB
$\mathcal{P}_{\mathsf{TX}}$	Transmitted power	30	30	30	dBm
F	Receiver noise figure	7	7	7	dB
ℓ	Coh. block size	500	500	500	(pure)

Table I collects parameters used to define the above three scenarios. In order to keep the number of parameters as low as possible, figures refer to the case of no absoprtion, *i.e.*, $v_1 = \cdots = v_{D_{\mathsf{W}}} = 1$. Bandwidths of interest lie in the interval 1 GHz–10 GHz. Attenuations in Table I are representative of communications towards outdoor users. In case the attenuation of a concrete wall is taken into account, the system would enter the low-SNR regime at smaller bandwidths than those of interest, and a fortiori our conclusions would be valid.

Figures 2 and 3 show rates (Mb/s) as a function of bandwidth $\mathcal{W}$ (Hz) for Case 1 and 2, respectively. Solid vs. dashed lines indicate capacity upper vs. lower bounds. Dotted lines indicate rates achieved via training. Peak constraints are either amplitude or fourth-moment constraints with $\beta = 3$. Curves refer to: AWGN upper bound C_{AWGN}; coherent upper bound C_{coh} from eq. (12); capacity upper bounds from eqs. (12) and (14), C_{UB} (there is no appreciable difference on plot between the two); capacity lower bound C_{LB} from eq. (19); rates achievable via training using truncated Gaussian inputs, $R^{\mathrm{tr}}_{\mathrm{TG}}$, and constant-modulus inputs optimized via block sharing, $R^{\mathrm{tr}}_{\mathrm{CM,opt}}$. Figure 2 refers to Case 1 (user near BS): the communication system operates in a relatively high SNR regime per degree of freedom (*e.g.* SNR is approximately equal to 3 dB when $\mathcal{W} = 1$ GHz). Capacity lower bound is almost overlapped to coherent capacity upper bound, and rates achievable using training and amplitude constrained inputs follow closely. It is shown, therefore, that dense signaling schemes are sufficient to achieve high rates in the order of Gb/s. Figure 3 refers to Case 2. The user approximately lies on the boundary of a circle that partitions the cell in two regions with same area: when users are placed uniformly at random, half of the users will perform better and the other half worse, on average, than the user on the boundary. In this case the

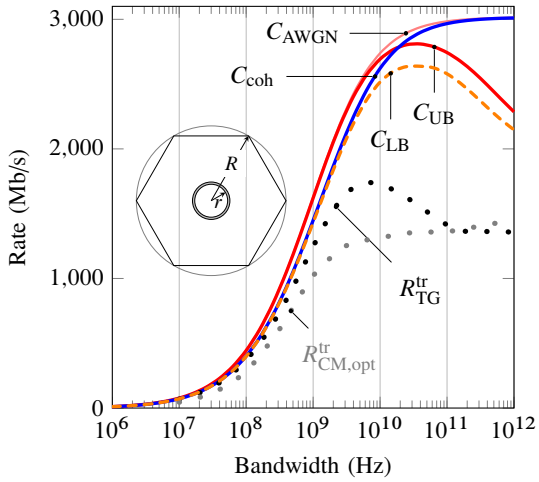

FIG. 2: Case 1: user near cell center (BS). Rate (Mb/s) as a function of bandwidth $\mathcal{W}$ (Hz). Scenario parameters: column "Case 1" of Table I.

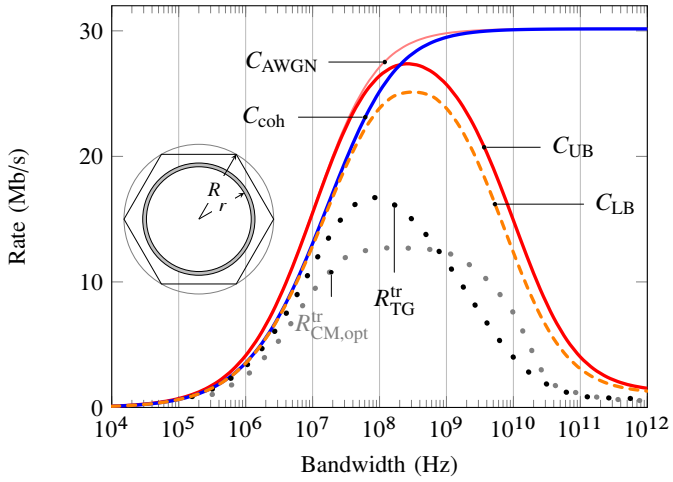

FIG. 3: Case 2: user in between center and edge. Rate (Mb/s) as a function of bandwidth $\mathcal{W}$ (Hz). Scenario parameters: column "Case 2" of Table I.

user is no longer in the high-SNR regime at bandwidths of interest (*e.g.* SNR is approximately equal to -16 dB when $\mathcal{W} = 1$ GHz), and capacity lower and upper bounds have negative slope. Although amplitude constrained inputs using training may experience a significant rate degradation, upper and lower bounds are close to each other, and also relatively close to the AWGN wideband capacity. We do not provide a figure for Case 3, which is qualitatively similar to Fig. 3: in this case, the user is located at a distance comparable to the typical mmWave cell radius, and communication occurs in the deep low-SNR regime. The AWGN wideband capacity is reduced due to strong attenuation and blockages, and further rate degradation is experienced by dense signaling schemes due to NLOS propagation.

Effect of other system parameters is investigated on Figs. 4 and 5, that refers to Case 2. Figure 4 shows capacity bounds as a function of bandwidth for weak ($|\mathsf{k}| = 0.25$) and strong ($|\mathsf{k}| = 0.75$) LOS scenarios. While insensitive for sufficiently small bandwidths, rate is particular dependent on the strength of the specular component in the wideband region. In particular, eq. (17) implies that an achievable wideband limit is $(1-p_{\text{B}})^2|\mathsf{k}|^2\mathcal{P}/\mathcal{N}_0$ nats/s, that corresponds to approximately 1.7 Mb/s for $|\mathsf{k}| = 0.25$ and to 15.3 Mb/s for $|\mathsf{k}| = 0.75$; eqs. (12) and (14) provide an upper bound wideband limit equal to $(1-p_{\text{B}})|\mathsf{k}|^2\mathcal{P}/\mathcal{N}_0$ nats/s, that corresponds to approximately 1.9 Mb/s for $|\mathsf{k}| = 0.25$ and to 16.9 Mb/s for $|\mathsf{k}| = 0.75$. Figure 5 shows capacity upper and lower bounds as a function of bandwidth for different block size $\ell \in \{10^2, 10^3, 10^4\}$. It is shown that, as block size grows, the wideband regime is pushed towards higher bandwidths, and the width of the frequency interval where each curve is above a fraction of the maximum increases as well. Bounds are approximately parallel for a large portion of the wideband regime, until reaching a value close to the wideband limit, which is not affected by the block size (upper and lower bounds tend to 1.20 Mb/s and 1.08 Mb/s, respectively).

VI. Discussion

Mobile communications using mmWave bands may have to operate in the wideband regime and experience low-SNR per degree of freedom, due to both large bandwidth and severe attenuation. Paired with NLOS propagation, that can occur even with small cell dimensions [3], and peak-constrained inputs, users may experience capacity limits far from the AWGN wideband limit.

We derived capacity upper and lower bounds as a function of bandwidth, LOS strength, blockage probability, and block size. Upper bounds are derived by adapting the work in [19] to block-fading and extending the bounding idea therein to address the case of kurtosis-constrained inputs. Lower bounds that are tight for a subset of parameters are proposed as well. We presented numerical results for a scenario where an outdoor user is located at different distances from the BS. As long as the user is sufficiently close to the BS, communication occurs in the high-SNR regime, and aside from technological issues of implementing orthogonal frequency-division multiplexing (OFDM) or similar systems with several thousand subcarriers [25], traditional (dense) signaling is nearly capacity-achieving. Rates may reach values in the order of Gb/s. However, a large fraction of users is not sufficiently close to the BS to operate in the high-SNR regime per degree of freedom: in this case, strong attenuation and blockages reduce the AWGN wideband limit, and NLOS propagation paired with dense signaling further degrades the achievable rate. We studied rate sensitivity to other system parameters, in particular strength of channel specular component and coherence block size. In the presence of LOS, the rate achievable with dense signaling is bounded away from zero, and tends to the rate of a system that uses the LOS component only. As the block size increases, communication enters the wideband regime at increasingly large bandwidth: however, we showed that for typical mobile communications block size and SNR regimes, dense signaling can partially cause the rate degradation.

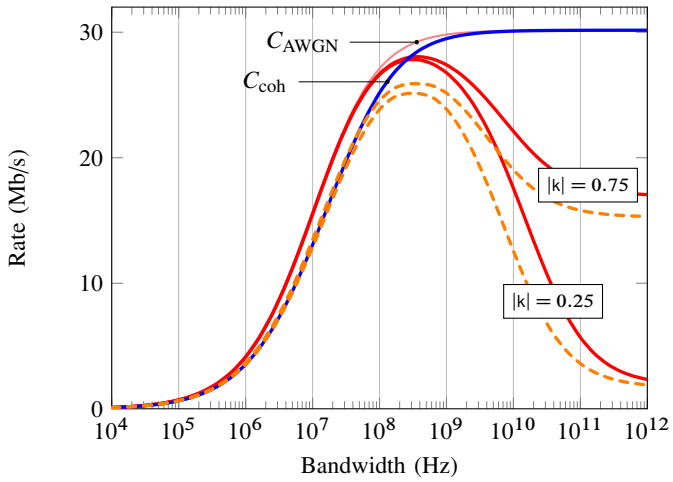

FIG. 4: Capacity upper bounds (solid line) and lower bounds (dashed line) as a function of bandwidth for different LOS component, $|\mathsf{k}| \in \{0.25, 0.75\}$.

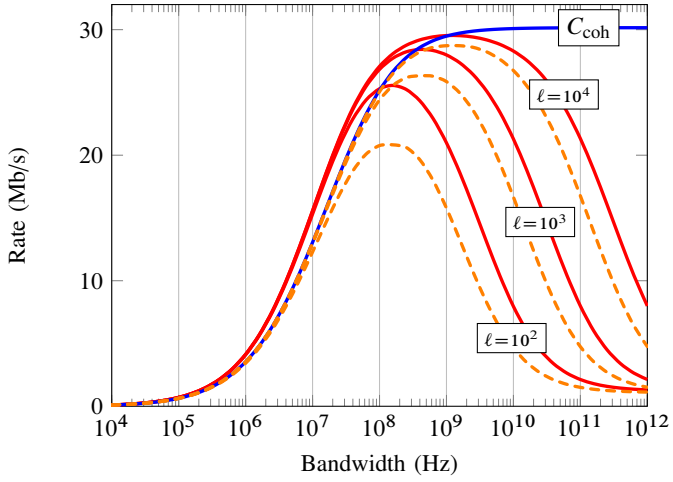

FIG. 5: Capacity upper bounds (solid line) and lower bounds (dashed line) as a function of bandwidth for different block sizes, $\ell \in \{10^2, 10^3, 10^4\}$.

Users may, therefore, experience both high- and low-SNR per degree of freedom within cells of relatively small radius such as mmWave cells. As a consequence, mmWave communications may have to support both dense and sparse signaling schemes in order to maximize the achievable rate for a given power expenditure. In particular, since both NLOS and low-SNR are strongly correlated, and also correlated with user distance from the BS, the rationale for the signaling should be the farther the user, the sparser the signaling. However, dense signaling can be sensibly used with either strong LOS or coverage that guarantees high-SNR per degree of freedom.

ACKNOWLEDGMENT

This work was supported in part by the SUTD-MIT Post-doctoral Programme, the SUTD-ZJU Research Collaboration under Grant SUTD-ZJU/RES/01/2014, and the MOE ARF Tier 2 under Grant MOE2014-T2-2-002.

REFERENCES

[1] J. Andrews, S. Buzzi, W. Choi, S. Hanly, A. Lozano, A. Soong, and J. Zhang, "What will 5G be?" *IEEE J. Sel. Areas Commun.*, vol. 32, no. 6, pp. 1065–1082, 2014.

[2] F. Boccardi, R. Heath, A. Lozano, T. Marzetta, and P. Popovski, "Five disruptive technology directions for 5G," *IEEE Commun. Mag.*, vol. 52, no. 2, pp. 74–80, 2014.

[3] M. Akdeniz, Y. Liu, M. Samimi, S. Sun, S. Rangan, T. Rappaport, and E. Erkip, "Millimeter wave channel modeling and cellular capacity evaluation," *IEEE J. Sel. Areas Commun.*, vol. 32, no. 6, pp. 1164–1179, 2014.

[4] T. Rappaport, S. Sun, R. Mayzus, H. Zhao, Y. Azar, K. Wang, G. Wong, J. Schulz, M. Samimi, and F. Gutierrez, "Millimeter wave mobile communications for 5G cellular: It will work!" *IEEE Access*, vol. 1, pp. 335–349, 2013.

[5] A. Sulyman, A. Nassar, M. Samimi, G. MacCartney, T. Rappaport, and A. Alsanie, "Radio propagation path loss models for 5G cellular networks in the 28 GHz and 38 GHz millimeter-wave bands," *IEEE Commun. Mag.*, vol. 52, no. 9, pp. 78–86, 2014.

[6] J. Pierce, "Ultimate performance of M-ary transmissions on fading channels," *IEEE Trans. Inf. Theory*, vol. 12, no. 1, pp. 2–5, 1966.

[7] R. Kennedy, *Fading Dispersive Communication Channels*. New York: Wiley-Interscience, 1969.

[8] M. Medard and R. G. Gallager, "Bandwidth scaling for fading multipath channels," *IEEE Trans. Inf. Theory*, vol. 48, no. 4, pp. 840–852, 2002.

[9] S. Verdú, "Spectral efficiency in the wideband regime," *IEEE Trans. Inf. Theory*, vol. 48, no. 6, pp. 1319–1343, 2002.

[10] T. Marzetta and B. Hochwald, "Capacity of a mobile multiple-antenna communication link in Rayleigh flat fading," *IEEE Trans. Inf. Theory*, vol. 45, no. 1, pp. 139–157, 1999.

[11] L. Zheng and D. Tse, "Communication on the Grassmann manifold: a geometric approach to the noncoherent multiple-antenna channel," *IEEE Trans. Inf. Theory*, vol. 48, no. 2, pp. 359–383, 2002.

[12] L. Zheng, D. Tse, and M. Medard, "Channel coherence in the low-SNR regime," *IEEE Trans. Inf. Theory*, vol. 53, no. 3, pp. 976–997, 2007.

[13] S. Ray, M. Medard, and L. Zheng, "On noncoherent MIMO channels in the wideband regime: Capacity and reliability," *IEEE Trans. Inf. Theory*, vol. 53, no. 6, pp. 1983–2009, 2007.

[14] V. Raghavan, G. Hariharan, and A. Sayeed, "Capacity of sparse multipath channels in the ultra-wideband regime," *IEEE J. Sel. Topics Signal Process.*, vol. 1, no. 3, pp. 357–371, 2007.

[15] V. Subramanian and B. Hajek, "Broad-band fading channels: signal burstiness and capacity," *IEEE Trans. Inf. Theory*, vol. 48, no. 4, pp. 809–827, 2002.

[16] A. Lapidoth and S. Moser, "Capacity bounds via duality with applications to multiple-antenna systems on flat-fading channels," *IEEE Trans. Inf. Theory*, vol. 49, no. 10, pp. 2426–2467, 2003.

[17] A. Lapidoth, "On the asymptotic capacity of stationary Gaussian fading channels," *IEEE Trans. Inf. Theory*, vol. 51, no. 2, pp. 437–446, 2005.

[18] V. Sethuraman and B. Hajek, "Capacity per unit energy of fading channels with a peak constraint," *IEEE Trans. Inf. Theory*, vol. 51, no. 9, pp. 3102–3120, 2005.

[19] G. Durisi, U. Schuster, H. Bolcskei, and S. Shamai, "Noncoherent capacity of underspread fading channels," *IEEE Trans. Inf. Theory*, vol. 56, no. 1, pp. 367–395, 2010.

[20] R. Gallager and M. Medard, "Bandwidth scaling for fading channels," in *Proc. IEEE Int. Symp. Inf. Theory*, 1997, p. 471.

[21] E. Telatar and D. Tse, "Capacity and mutual information of wideband multipath fading channels," *IEEE Trans. Inf. Theory*, vol. 46, no. 4, pp. 1384–1400, 2000.

[22] K. Liu, T. Kadous, and A. Sayeed, "Orthogonal time-frequency signaling over doubly dispersive channels," *IEEE Trans. Inf. Theory*, vol. 50, no. 11, pp. 2583–2603, 2004.

[23] A. Lozano, A. Tulino, and S. Verdu, "Optimum power allocation for parallel Gaussian channels with arbitrary input distributions," *IEEE Trans. Inf. Theory*, vol. 52, no. 7, pp. 3033–3051, 2006.

[24] ——, "Optimum power allocation for multiuser OFDM with arbitrary signal constellations," *IEEE Trans. Commun.*, vol. 56, no. 5, pp. 828–837, 2008.

[25] D. Porrat, D. Tse, and S. Nacu, "Channel uncertainty in ultra-wideband communication systems," *IEEE Trans. Inf. Theory*, vol. 53, no. 1, pp. 194–208, 2007.